CHAPTER VII

DISCUSSION

7.1 The DACCT Measurement

For the semiconductor which have no reliable ohmic contact, such as p-$CuInSe_2$, there is a simple measurement technique, i.e. DACCT, which is appropriate to measure a small barrier of the ohmic contact itself. The technique clearly shows the existence of the small barrier, as can be seen in Fig.7 and Fig.8, since the barrier resistance does depend on the injecting contact area while the bulk resistance does not. So, whenever the DACCT voltage split into upper and lower branches, the difference is clearly due to the barrier. Au/p-$CuInSe_2$ and Ni/p-$CuInSe_2$ are examined using DACCT. This technique should also be appropriate for other semiconductors on which ohmic contacts are difficult to make.

The DACCT can separate the bulk and the barrier effect and show the bulk properties at temperatures warmer than the "split" temperature which can cover a large range depending on the current. Because our instrument is not suitable for such investigation interested readers are invited to read the original works (Tantraporn, 1970; Tantraporn, 1972; Tantraporn, 1980).

7.2 The Pseudo-Richardson Model

a) To illustrate the idea of the pseudo-Richardson model, we calculate the V-T dependence at constant reverse current by :

1) using only thermionic, i.e. neglect tunneling contribution of hole below B_{max} ;

2) both thermionic - field, i.e. both contribution of hole above and below B_{max} ;

3) neglecting thermionic, i.e. neglect contribution of hole above B_{max}. The results are shown in Fig. 18.
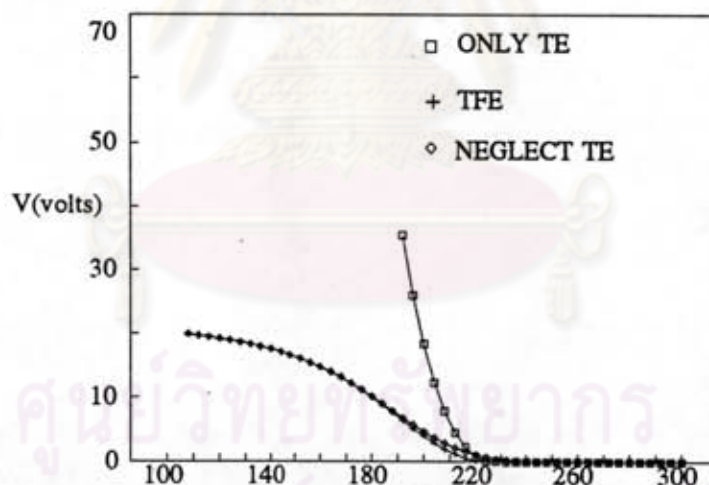

Fig.18 The calculated reverse voltage as a function of temperature at constant current (0.1 mA) by assuming only thermionic emission (only TE), thermionic-field emission (TFE), or only tunneling (neglect TE). The temperature value at which the voltage start to increase significantly in the case TFE is slightly lower than those for the other two cases. The parameters used in calculation are $\phi = 0.5$ eV, $\Delta = 0.1$ eV, $m^+ = 1$, $N_a(b) = 1 \times 10^{17}$ cm^{-3}, $N_a(s) = 1 \times 10^{20}$ cm^{-3}, $\alpha = 0.15$ /^{o}A, $A_{app} = 1 \times 10^{-2}$ cm^2, density of state effective mass = 1, and dielectric constant = 10.

For TFE, upon cooling, the temperature that the voltage start to increase ,i.e. the split temperature is lower which correspond to smaller B_{eff} than the other two. Thus pseudo-Richardson model assumed as if there is only one conduction mechanism, i.e. thermionic emission, other possible conduction mechanisms are absorbed by the reduction of the barrier to be B_{eff}. Note that this model works even most of the current due to tunneling component , as can be seen by compare TFE and neglected TE in Fig. 18 which is nearly the same.

In any case the definition of the split temperature and the determination of the effective barrier height using the pseudo-Richardson equation discussed in the section 3.2 are valid and very useful. The ohmic criterion in the section4.2 is reasonable. It is defined regardless the dimension of the bulk. More importantly both contacts of different areas, or combination of identical dot contacts of the same area, can be fabricated on the same surface, not only simplifying sample preparation, but also allowing more definitive determination of the "bulk" part of the lower branch at temperatures lower than the split temperature. In addition, it is a relatively easy experiment, which can clearly seperate the bulk and barrier effect. Other reported techniques do not offer the clear separation.

b) When comparing the experimental value of $R_c(prm)$ with R_t in Table5 , one can see that $R_c(prm)$ is properly bound. The source of error of $R_c(prm)$ should be $A_{eff} A^*$ which may contain a substantial percentage error due to graphical extrapolation and the logarithmic nature of the Richardson plot. However, in some cases $R_c(prm)$ is found larger than R_t, indicating some error in either $R_c(prm)$ or R_t measurement.

Table 10 below shows the comparison between A_{app} and $A_{eff} A^*$. In this table, the small A_{app} correlates well with the small $A_{eff} A^*$. Since A_{app} depends on the insulator thickness, as seen in eq. 4.3.2.1. However, in the pseudo-Richardson model A_{eff} and A^* appear in compound form which could not be separated from each other. As pointed out earlier some degree of tunneling effect is contained in $A_{eff} A^*$.

TABLE 10

Comparison between A_{app} and $A_{eff} A^*$ for Au /p-CuInSe$_2$

#contact	A_{app} (cm^2)	$A_{eff} A^*$ (A/K^2)
B4/9/2	7.72×10^{-3}	1.2×10^{-2}
C3/16/1	4.67×10^{-3}	2.0×10^{-3}
B4/9/1	3.07×10^{-3}	2.9×10^{-3}
C3/20	2.32×10^{-3}	3.3×10^{-4}
B6/3/1	1.33×10^{-3}	1.6×10^{-3}
D3/4	9.78×10^{-4}	8.1×10^{-4}
D3/5/1	6.99×10^{-4}	8.0×10^{-4}
B6/4	6.40×10^{-4}	1.9×10^{-3}
B4/12/1	6.10×10^{-4}	4.8×10^{-4}
B4/12/2	1.77×10^{-4}	4.3×10^{-5}
C3/16/2	1.61×10^{-4}	6.3×10^{-4}

#contact	A_{app} (cm^2)	A_{eff} A* (A/K^2)
B4/12/2	1.77×10^{-4}	4.3×10^{-5}
C3/16/2	1.61×10^{-4}	6.3×10^{-4}
B4/11/4	1.11×10^{-4}	2.1×10^{-5}
D3/5/2	8.32×10^{-5}	8.3×10^{-4}
B3/5	4.95×10^{-5}	8.6×10^{-4}
B6/3/2	2.20×10^{-5}	1.8×10^{-5}
C3/19	8.03×10^{-6}	3.4×10^{-4}
B4/11/1	3.48×10^{-6}	4.3×10^{-6}
B4/11/2	3.09×10^{-6}	7.1×10^{-6}
B4/11/5	2.28×10^{-6}	1.3×10^{-6}
B4/11/3	9.23×10^{-7}	3.2×10^{-6}

7.3 The Ohmic Range of the Best Au/p-CuInSe$_2$ Contact

From A_{eff} A* and B_{eff} in Table 5, one can calculate the I, V and T combination at which the contact becomes blocking. According to the section 4.2, a contact is not ohmic (blocking) when the current used in measurement exceeds the Richardson current. One then expects to encounter with barrier effect in measuring bulk properties.

As an illustration ,#B4/12/1 which shows the least R_c(prm) in Table5 is selected. We believe that this is the best of the ohmic contact of p-CuInSe$_2$. The effective barrier B_{eff} of this contact, from Table 5, is 0.200 eV. The geometrical contact area 9.5×10^{-3} cm^2 which correspond to A_{eff} A* = 4.8×10^{-4} A/K^2 in Table 5. If one, however, uses the contact area, say, 4.75×10^{-3} cm^2 in measurement, the Richardson current I_{Rich}, at temperature T, according to eq. 4.1.1 should be :

$$I_{Rich} = 2.4 \times 10^{-4} \, T^2 \, \exp(-0.200 \, /kT) \qquad \text{A.}$$

Suppose that one used current 200×10^{-6} A in this measurement, according to above equation, the temperature that this contact becomes blocking is about 213 K. At temperature lower than 213 K , at this current, one would in fact already encounter the barrier effect. This shows that, even our best contact at not too high current density, i.e. about 2×10^{-2} A/cm^2, cannot safely be regarded as ohmic contact at 213 K, not too far from room temperature.

Using a current larger than the Richardson current in an experiment designed to determined the bulk's activation energy, the activation energy value obtained may in fact be the barrier effect. The value of B_{eff} in Table 5 happens to be comparable to deep impurities levels in most solids. So, one must be careful in measuring the value of the bulk's activation energy in this energy range.

7.4 General Discussion of the Fitting Process

a) In fitting procedure, the effect of unknown conduction area is reduced by normalized the experimental data with a data point, call base. This base get higher statistical weight than other data points, and the accuracies in the resultant fitting parameters depend on this base. For example, if for some reason the voltage of the base is larger than it should be due to an experimental error, while the other data points are correct. The fitting parameters tend to give the barrier shape which is too low and too thin than it should be. That is, ϕ tends to be too low, Δ tends too low, etc. Consequently, A_{app} tends to be too small.

In principle, one should give equal weight to every data point and obtain A_{app} as one more direct fitting parameter, i.e. not normalized by the base. But this may add to the overall system error; more parameters give larger total error. Furthermore, it consumes so much more computer time as to make the attempt unjustified.

The valid split voltage is obtained when the lower branch voltage is still due to the "bulk" ie., the larger contact is still not blocking. The lower branch should not show rapid increase, i.e. unlike Fig.18. Of all the data, we

choose intermediate current and temperature with large range in the graph, as the base in Table6 and 8. All data in Table 7 are chosen on this basis.

b) For some contacts, A_{app} have nearly equal to the electrode area. For example : the A_{app} of #B4/9/2 is 7.72×10^{-3} cm^2 nearly equal to 9.5×10^{-3} cm^2 which is the electrode area. According to the "electrode area testing" of Tantraporn (1972), the physical reality test is met and the fitting parameters should have physical significance.

However, according to Fig. 4, only three parameters, ϕ , m^+ and $N_a(b)$ are regarded as significant parameters from fitting, as we found that these parameters do not change too much when other different initial parameters are used for fitting. From the other different measurements, the same values of these parameters should be obtained.

c) Normally, A_{app} should be smaller than the geometrical contact area because of the edge effect, pin hole, patchiness, and a thin series insulator. However, in this work, the latter should be pertinent. We speculate the existence of a thin insulator inbetween the metal and the semiconductor for the case of smaller A_{app}, as discussed earlier.

7.5 The Significant Barrier Parameters for Au/p-CuInSe$_2$

According to the section 4.3.1 and 7.4.b, the three significant barrier parameters of Au/p-CuInSe$_2$ that were obtained from fitting are :

The barrier height ϕ ranging from 0.3608 - 0.5680 eV. The value of barrier height of Au/p-CuInSe$_2$ as reported by Nelson et. al. is 0.6 eV. However, it is only one value, and is hard to compare with our result.

The doping concentration $N_a(b)$ ranging from $1.09\text{-}7.99\text{x}10^{17}$ cm^{-3}. These values are the same order of the values in Table 1 which were obtained from Hall measurement. However, the present of Au may be modify the doping concentration.

The tunneling effective mass m^+ ranging from 0.0565 - 0.1698. Since the effective mass of light and heavy hole of p-CuInSe$_2$ are 0.092 and 0.73 respectively, the light holes appear to contribute more than the heavy holes in tunneling. We consider this fitting result as a confirmation of the influence of light hole in the TFE conduction.

It is interesting to note that in eq. 4.3.2.3 m^+ occurs as a product with $[B(x;V) - E]$ derived from the WKB model with the profile of $B(x;V)$ obtained from integrating the one dimensional Poisson equation. Therefore, m^+ can absorb the non one-dimensional effects in the case that the metal-semiconductor interface is not an infinite, flat, plane. Nature is kind. The real

surface is very non-ideal in the microscale and yet the one dimensional WKB model suffices.

7.6 The Expectation Value of the Lowest Contact Resistivity of Near Stoichiometry p-CuInSe$_2$

For Au/p-CuInSe$_2$, heat treatment in hydrogen atmosphere (about 300-400 °C), most contacts become high resistive contacts. Even with deposited Au on preheated p-CuInSe$_2$ in vacuum chamber (about 250 °C), all contacts have high contact resistivity (in the order of 10^0 Ω-cm^2).

For Ni/p-CuInSe$_2$, heat-treated similarly at 450 °C, the contacts become slightly blistered but the contact resistance did not change much (within the same order of magnitude). These heat treatments were performed in the early days of trying to achieve ohmic contact, and were not carried out systematically. However, it indicates that the ohmic contact (for bulk properties measurement) of p-CuInSe$_2$ probably cannot be obtained from traditional process, i.e. by heat diffusion of the metal.

Both Au and Ni-type contacts after heat treatment gave unsteady signal in DACCT measurement. They also show unexpected pattern, i.e. did not look like Fig.7 and 8, which were the results of careful experiment. This could be due to trap-related effects. We at this time cannot interpret the data with unsteady signals. Other high resistance contacts also show similar effect.

It is worthwhile to note that in the early stage of trying to make ohmic contact of Au/p-CuInSe$_2$, more than a hundred contacts were rejected because they yielded unsteady behaviors and /or they didnot yield a clear splitting DACCT pattern.

For Au/p-CuInSe$_2$, there is a golden rule in fabrication of an ohmic contact. That is to avoid high temperatures as much as possible, otherwise one usually gets high resistance contact.

The value of R$_c$(fit) in the section6.2.2 is not a true contact resistance, it is the theoretical dV/dI at I~0 due to the barrier only, and hence should be the lower limit of the experimental value of the contact resistance measurement. This can be seen by compare R$_{approx}$ of #B4/11/3 in Table 4 with R$_c$(fit) in Table 9, i.e. 0.84 and 0.39 Ω. The reader is however reminded of the fuzziness of the definition of R$_{approx}$ (p.60). When multiplies R$_c$(fit) with contact area one get ρ_c(fit) which is the lower limit of the contact resistivity. Since Au is the best metal for the ohmic contact of p-CuInSe$_2$ and our substrates are near stoichiometry, we claim that the value of the lowest contact resistivity of near stoichiometry p-CuInSe$_2$ should not be lower than the order of 10^{-3} Ω-cm^2, at room temperature. Note that this value is not too far from 0.06 Ω-cm^2, the acceptable back contact for solar cells.

7.7 The Decrease in the Doping Concentration Near the Interface of Some Au/p-CuInSe₂ Contacts

Some Au contacts show the pattern similar that of the curve in Fig.19, the voltages appears to continue upward at high voltage even at low temperature. The pattern is different from TFE pattern in Fig. 18.
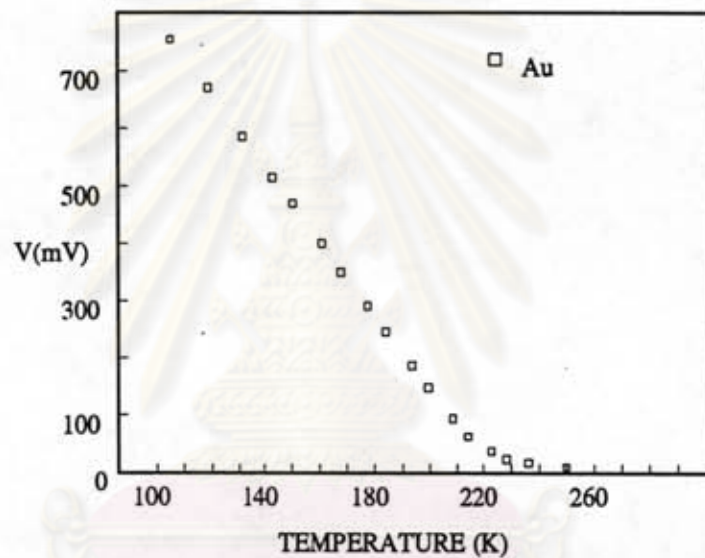

Fig.19 Sample of the pattern of the decreasing of the doping concentration of some Au/p-CuInSe₂ contacts. The constant current of the V-T characteristic in this figure is 1.03 mA.

At a given constant current, when the temperature decreases, the barrier conduction needs a larger applied voltage, i.e. higher electric field near the interface is needed to sustain the continuity of current. For the same junction electric field, according to Poisson equation, low doping concentration needs

more voltage than high doping. So, the pattern in Fig. 19 should be because as the distance is far from the interface, the doping concentration decrease.

7.8 The Effect of Nonhomogeneity in a Substrate

Among the different composition of p-CuInSe$_2$ used and crude method of electroding, there is no observable tendency which one would always obtain good ohmic contact. This does not exclude the possible dependence on the composition of the substrates; the effect due to different compositions in the contacted layer may be masked by the variations in the crystal substrate available.

On a large sample, i.e. #B4/11 on which we can fabricate five Au contacts, it was observed that the contact resistivity depend on position, i.e. first-freeze portion yields smaller contact resistivity than the last-freeze. To reconfirm this effect, we refabricated three contacts of Au of equal areas, i.e. 9.5×10^{-3} cm^2 from the first to the last freeze, the total resistance were 0.98, 2.54 and 4.13 Ω respectively, the same trend.

This may not adequately establish that first-freeze portion will always yield better contacts than last-freeze does. More experiment should be performed.

7.9 The Mo/p-CuInSe$_2$ Contact

For as-deposited Mo/p-CuInSe$_2$ contacts, because of their relatively high resistance, there exists perhaps a homojunction. A homojunction is characterized

as a high voltage low current devices (a p-n junction blocking the injection), while a Schottky junction is a low voltage high current device (Rhoderick, 1978). In the case of the Mo contact, our results are in agreement with Toro's (i.e. high resistance contacts) which indicate a homojunction. Note that Mo was deposited by sputtering. The kinetic energy of Mo is released to p-CuInSe$_2$ in the form of heat and could convert the type of semiconductor in the near-surface region. The mechanism involved could be Se out-diffusion (Toro, 1986).

Heat treatment of Mo/p-CuInSe$_2$ contacts, as can see in Table 3, also causes the same trend as in Toro's work, the contact resistivity is reduced. However, it still gave unsteady signal in the DACCT measurement.

7.10 The Anti-Richardson Behavior of the Ni/p-CuInSe$_2$ Contact

(In this section, the energy means electron energy.)

The split voltages at high current and low temperature of Ni/p-CuInSe$_2$ contact showed an interesting feature. In this range, the split voltages at low temperature and constant current, is lower than at the higher temperature, contrary to expected behaviors of the TE and TFE mechanisms. We called this "anti-Richardson behavior", since the resistance of the contact increases with temperature. It indicates that some refinements are needed in the theoretical models used in explanation Ni/p-CuInSe$_2$ contact. At this stage, we are not yet successful in explaining this effect.

However, the following argument may be the answer to the question.

Let us be, for the time being, interested only in the temperature, ie. ignore the influence of the doping concentration. As the temperature decreases, the mechanisms that dominate in the current conduction are thermionic, thermionic-field, and field emission, respectively. These are the well known situations. We are interested in the last case, the field emission, in which the significant part of the current come from the flux above the metal's Fermi level.

Normally, in calculating the current density across the Schottky barrier, one consider two fluxes of the carrier in opposite directions. For example, the fluxes of electron from the semiconductor to the metal and vice versa. However, in the reverse bias of p-type semiconductor, if the bias is large enough, as in the case of the anti-Richardson behavior, the flux from metal to semiconductor can be neglected, and the current is limited by the number of unoccupied states in the metal side.

As the temperature decreases, the states in metal side below the metal Fermi level have increasing probability of being filled with electrons, but the states above the Fermi level have decreasing. probabilty. When electrons from the semiconductor side tunnel through the barrier to the metal side, at the energy below the metal Fermi level, they found fewer number of the unoccupied states available, but with opposite situation for the energy above the metal Fermi level. So, as the temperature decreases, the electron flux in the energy range below the metal Fermi level become less significant, while the flux above the Fermi level become more significant.

There may be a situation that at given bias and low temperature, the main parts of the significant flux lie above the metal Fermi level. In this case, if the number of states above the metal Fermi level is large enough, as the temperature decreases, the number of unoccupied states increases. Since, the reverse bias voltages shift energy of the electrons in the semiconductor side upward, as can see in figure 22, so, if the bias is large enough, the energy range near the metal Fermi level lie deep below the semiconductor Fermi level. As a result, the flux of electrons in the semiconductor side at this energy range do not vary much with temperature. In short, as the temperture decreases, the source of electrons does not significantly decrease, while the sink significantly increases. So, the current, at given bias, may increase, provided that the barrier's shape should look like oxide's, and because of this barrier shape, the transmission coefficient doest not increase as much with energy.

The above desciption may be seen in the following crude calculation.

For simplicity, we used the rectangular barrier shape and assumed that the barrier shape is independent from the bias. The barrier under reverse bias,is shown in figure 20.
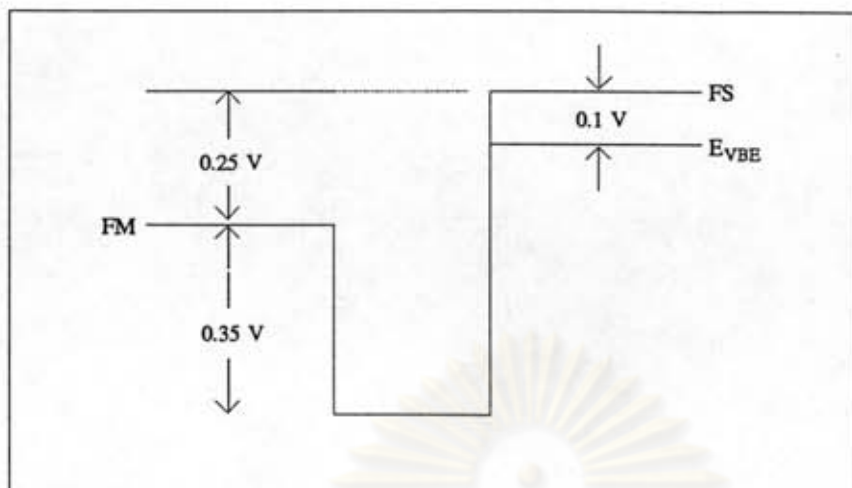
Fig.20 The rectangular barrier of p-type semiconductor under reverse bias.
FM, FS and E_{VBE} are metal Fermi level, semiconductor Fermi level and
valence band edge of the semiconductor, respectively.

Setting the metal Fermi level as zero, the flux distribution of the
electrons that incident in the x-direction normal to the barrier in the
semiconductor side, under the reverse bias V, is given by, see for example
Fowler(1955) :

$$F_S(V,T;E_x) = \frac{4\pi m^* kT}{h^3} \ln\{1 + \exp{-(E_x - qV)/kT}\} \qquad 7.10.1$$

where m* is the effective mass of electron in the semiconductor, the others
symbols are as usual.

At a given energy, the differential current density from semiconductor
to metal may be :

$$dJ_{sm} = C F(V,T;E_x) D(E_x) [1-f_m(E_x)] P_m(E_x) dE_x \qquad 7.10.2$$

where

$D(E_x)$ is the transmission coefficient

$f_m(E_x)$ is the Fermi-Dirac distribution function in the metal

$P_m(E_x)$ is the density of states in the metal

C   is the constant which set the dimension of the above
equation equal to the current density.

We will set the magnitude of C equal to unity. For the s-band, the magnitude of $P_m(E_x)$ may equal to unity.

Note that equation 7.10.2 is not exactly correct. Because the Fermi-Dirac distribution function depends on the total energy, not the energy in the x-direction. The density of states in the metal may also be incorrect in this sense.

The situation is very complicate if one consider the flux distribution from metal to semiconductor. However, as already mentioned, we consider only large enough bias where this flux can be neglected.

So, the total flux may be :

$$J_{sm} = \int_0^{V-\Delta} F(V,T;E_x)D(E_x)\{1 - f_m(E_x)\}P_m(E_x)dE_x \qquad 7.10.3$$

The transmission coefficient $D(E_x)$ will be calculated from eq.4.3.2.3.

Table 11 below shows the flux distribution at 100 and 200 K, the effective mass of the semiconductor m* and the tunneling effective mass in eq.4.3.2.3 are set to 1 and 0.1, respectively. The barrier hight and the barrier width are -0.35 eV and 30 angstroms. The different between the

semiconductor Fermi level and the valence band edge is 0.1 eV, the bias is 0.25 volts. The density of states $P_m(E_x)$, assume to be constant, at 20. The incremental of the energy dE_x is 0.005 eV.

TABLE 11

Flux distribution of rectangular barrier at 100 and 200 K.

E	$\ln(dJ_{sm}$ at 100 K)	$\ln(dJ_{sm}$ at 200 K)
(eV)	$\ln$(particles/cm^2 sec)	$\ln$(particles/cm^2 sec)
-0.345	-16.7690	23.2568
-0.340	-15.8915	23.5507
-0.335	-14.9606	23.9092
-0.330	-13.9900	24.3011
-0.325	-13.0011	24.7143
-0.320	-11.9919	25.1426
-0.315	-10.9720	25.5824
-0.310	-9.9426	25.5888
-0.305	-8.9067	26.4873
-0.300	-7.8640	26.9497
-0.295	-6.8161	27.4172
-0.290	-5.7638	27.8893
-0.285	-4.7076	28.3653
-0.280	-3.6478	28.8449
-0.275	-2.5849	29.3275
-0.270	-1.5192	29.8130
-0.265	-0.4510	30.3010
-0.260	0.6195	30.7912
-0.255	1.6921	31.2836
-0.250	2.7666	31.7779

E (eV)	ln(dJ$_{sm}$ at 100 K) ln(particles/cm^2 sec)	ln(dJ$_{sm}$ at 200 K) ln(particles/cm^2 sec)
0.255	1.6921	31.2836
-0.250	2.7666	31.7779
-0.245	3.8429	32.2740
-0.240	4.9209	32.7718
-0.235	6.0004	33.2710
-0.230	7.0813	33.7717
-0.225	8.1635	34.2737
-0.220	9.2469	34.7769
-0.215	10.3315	35.2813
-0.210	11.4172	35.7867
-0.205	12.5039	36.2932
-0.200	13.5916	36.8006
-0.195	14.6801	37.3089
-0.190	15.7695	37.8181
-0.185	16.8597	38.3280
-0.180	17.9506	38.8387
-0.175	19.0423	39.3501
-0.170	20.1346	39.8622
-0.165	21.2275	40.3749
-0.160	22.3211	40.8882
-0.155	23.4152	41.4020
-0.150	24.5099	41.9163
-0.145	25.6051	42.4312
-0.140	26.7007	42.9464
-0.135	27.7968	43.4621
-0.130	28.8933	43.9781
-0.125	29.9903	44.4945
-0.120	31.0876	45.0111
-0.115	32.1852	45.5279

E (eV)	ln(dJ$_{sm}$ at 100 K) ln(particles/cm^2 sec)	ln(dJ$_{sm}$ at 200 K) ln(particles/cm^2 sec)
-0.120	31.0876	45.0111
-0.115	32.1852	45.5279
-0.110	33.2832	46.0448
-0.105	34.3815	46.5617
-0.100	35.4801	47.0786
-0.095	36.5789	47.5952
-0.090	37.6780	48.1114
-0.085	38.7773	48.6269
-0.080	39.8768	49.1414
-0.075	40.9764	49.6545
-0.070	42.0761	50.1657
-0.065	43.1757	50.6742
-0.060	44.2751	51.1791
-0.055	45.3739	51.6792
-0.050	46.4717	52.1730
-0.045	47.5675	52.6585
-0.040	48.6597	53.1333
-0.035	49.7453	53.5945
-0.030	50.8195	54.0383
-0.025	51.8738	54.4607
-0.020	52.8942	54.8572
-0.015	53.8589	55.2231
-0.010	54.7375	55.5541
-0.005	55.4941	55.8463
-0.000	56.0973	56.0973
0.005	56.5344	56.3063
0.010	56.8180	56.4741
0.015	56.9795	56.6031
0.020	57.0548	56.6969
0.025	57.0743	56.7600

E	ln(dJ$_{sm}$ at 100 K)	ln(dJ$_{sm}$ at 200 K)
(eV)	ln(particles/cm^2 sec)	ln(particles/cm^2 sec)
0.020	57.0548	56.6969
0.025	57.0743	56.7600
0.030	57.0596	56.7970
0.035	57.0247	56.8122
0.040	56.9780	56.8099
0.045	56.9245	56.7935
0.050	56.8669	56.7659
0.055	56.8069	56.7297
0.060	56.7452	56.6865
0.065	56.6825	56.6380
0.070	56.6188	56.5853
0.075	56.5544	56.5292
0.080	56.4893	56.4703
0.085	56.4235	56.4092
0.090	56.3569	56.3462
0.095	56.2895	56.2815
0.100	56.2213	56.2153
0.105	56.1521	56.1477
0.110	56.0820	56.0787
0.115	56.0107	56.0083
0.120	55.9383	55.9365
0.125	55.8646	55.8633
0.130	55.7895	55.7885
0.135	55.7128	55.7121
0.140	55.6343	55.6340
0.145	55.5540	55.5539
ln(J$_{total}$)	59.9685	59.8811

where J_{total} in the last line is the total flux at each temperature. It shows that, at this bias, the current density at low temperature is greater than at high temperature.

Although the above calculation is over simplified, it however indicates possible mechanisms leading to the anti-Richardson behavior. Note that, for Ni, there is a large density of states of the d-band above the Fermi level (Mattheiss, 1964), while the d-band of Au is filled. This may be the reason that, for Ni, there is the anti-Richardson behavior, while the behavior is not observed for Au.

By AES analysis, Toro reported the presence of oxygen throughout the Ni layer of Ni/p-CuInSe$_2$ contact. This may support the blunt barrier shape of Ni/p-CuInSe$_2$, as in the above discussion.

All of the description and the calculation in this section are merely to give the feeling of one possible answer of the anti-Richardson behavior. Of course, more rigorous theoretical calculations and experiments should be performed. Further study of the anti-Richardson behavior is beyond the scope of the present thesis, and is left as a future pursuit.